



ChemTech

## International Journal of ChemTech Research

CODEN (USA): IJCRGG, ISSN: 0974-4290, ISSN(Online):2455-9555  
Vol.11 No.09, pp 308-321, 2018

### Study on Structure, Vibrational assignment, NBO- Analysis, HOMO-LUMO, and Molecular Docking of D-Pinitol

A. Manikandan<sup>1\*</sup>, P. Rajesh<sup>2</sup>, T. Gnanasambandan<sup>3</sup>, A.R. Prabakaran<sup>1</sup>

<sup>1</sup>Department of Physics, Spectrophysics Research Laboratory, Pachaiyappa's College, Chennai – 600 030, India.

<sup>2</sup>Department of Physics, Apollo Arts and science college, Chennai- 600078, India.

<sup>3</sup>Department of Physics, Siddharth Institute of Science and Technology, Puttur- 517583, India.

**Abstract :** The plant source based on natural material products cover a major sector of the biomedical and medical field then the focus on plant research has been increased worldwide. We have performed a structural investigation and spectroscopic studies of a natural plant material product cyclitol: D-Pinitol. The spectroscopic properties of D-Pinitol were analyzed in the present study using FT-IR, FT-Raman spectra in the region of FT-IR (4000-400cm<sup>-1</sup> and FT-Raman cm<sup>-1</sup>). The vibrational frequencies were obtained by DFT-B3LYP/-311++G(d,p) as a basis set. The optimized geometry of D-Pinitol has been elucidated using, vibrational assignment and calculation of potential energy distribution (PED). The charges of atoms and electronic structural system NBO/NLMO. The molecular electrostatic surface and reactivity of this natural molecule have been calculated. The UV-Vis spectrum has been recorded in methanol solvent (MeOH) and electronic properties such as frontier orbitals (FMOs) calculated HOMO-LUMO is measure by the TD-DFT approach. Docking simulation is powerful way to figure out the binding structure of a substrate in its receptor.

**Key Words :** PED, NBO, FMOs, Docking Study.

#### 1. Introduction:

D-Pinitol, IUPAC name D-3-O-methyl-chiro-inositol, is a cyclitol occurring in nature compound. The cyclitols are extensively distributed in the plant kingdom. The D-pinitol(C<sub>7</sub>H<sub>14</sub>O<sub>6</sub>) in especially 3-O- methyl ether is widely distributed but D-Chiro-inositol is originated in plants. In the occurrence of most great quantities of myo-inositol, inconsequential amount of D-Chiro-inositol have been indicated in animal and human tissue. Inositol stands for 1,2,3,4,5,6-cyclohexanehexol and consists of nine discrete stereoisomers, namely, cis-, myo-, allo-, muco-, neo-, epi-, scyllo-, optical isomer p-chiro -, and L-chiro-inositol. D-Pinitol is one of the naturally occurring inositol derivatives[1]. This lower-molecular-weight, non-toxic, sugar like compound is biodegradable[2,3] and has the food supplement because of its reported effectiveness in lowering blood glucose level. The worldwide total number of people with diabetes is projected to upswing from 171 million in 2000 to 366 million in 2030.

A. Manikandan *et al* /International Journal of ChemTech Research, 2018,11(09): 308-321.

DOI= <http://dx.doi.org/10.20902/IJCTR.2018.110937>

D-Pinitol is a bioactive compound re-counted to have important biological and medical activities. The secondary metabolism exerts medical activities on insulin-like, human metabolism [4], antitumor, anti-inflammatory[5,6], osmoprotectant[7], embryo development[8], cardioprotective[9], antihyperlipidemic[10]. This compound also has some bio control effect on lardvicidal activities, mothy ovipositor attraction butterfly. Literature survey reveals that so far there is no completespectroscopic study FT-IR, FT-Raman, and quantum chemical calculation study for tittle compound D-Pinitol. In this study, we set out the experimental and theoretical investigation of the conformation, vibrational and electronic transition of D-Pinitol. The optimized geometry parameters, fundamental frequencies, molecular frontier orbitals surfaces(FMOs), molecular electrostatic potential (MEP) of the tittle compound have been calculated by using DFT–B3LYP method 6-311++G(d,p) basis set to explore the molecular dynamics and structural parameters that govern the chemical calculations behavior and to compare predictions made from theory with experimental observations.

## 2. Experimental Details

The compound D-Pinitol(> 90 % (HPLC), powder)was purchased from Sigma–Aldrich Chemical Company, USA and used as such without further purification to record FT-IR and FT- Raman spectra. The FT-IR spectrum of the title compound was recorded in the 4000–400  $\text{cm}^{-1}$  region with a BRUKER IFS 66 V spectrometer using KBr pellets. The FT-Raman spectrum was also recorded in the region 4000 - 100  $\text{cm}^{-1}$  with BRUKER IFS 100/s Raman molecule equipped with Nd: YAG laser source operating at 1064 nm line width 150mWpower. The ultraviolet absorption spectrum of sample solved in methanol was examined in the range 200–400 nm by using Cary 5E UV–Vis NIR recording spectrometer.

## 3. Quantum Chemical Calculations

Calculations of the title compound were carried out with Gaussian03W software program [11] using the B3LYP/6-311++G(d,p)quantum chemical calculation methods to predict the molecular structure and vibrational wavenumbers. Calculations were accepted out with Becke's three parameter hybrid model using the Lee–Yang–Parr correlation functional (B3LYP) method. In order to interpret various second order interaction between the filled and empty orbitals, NBO calculations are doneby Gaussian03W package at the DFT/B3LYP/6-311++G(d,p) level. NBO analysis provides an efficient method for studying inter and intramolecular bonding and interaction among bonds. The UV–Vis range, electronic transitions, vertical excitation energies and absorbance of the title molecule are calculated with the TD-DFT. The electronic transitions such as the highest occupied molecular orbital (HOMO) and lowestlying unoccupied molecular orbital (LUMO) energies are computed with DFT method. The assignments of each vibration were examined on the basis of the measured data and potential energy distribution (PED) of the vibrational modes that carried out by VEDA 4.0 program [12]. The assignment of the calculated wavenumbers is aided by the animation option of Gauss view program, which gives a visual presentation of the vibrational modes [13].

## 4. Results and Discussion

### 4.1 Ground State Structure Analysis

The optimized molecular structure of D-Pinitol belongsto  $C_1$  point group symmetry. The optimized parameters such as bond length and bond angle are compared with the obtainable experimental X-ray diffraction (XRD) data of the tittle compound structure so as to calculate the close consistency of those parameters [14] and show good agreement with each other parameters are presented of tittle compound calculated by B3LYP/6-311++G(d,p) basis set **Table 1**.The magnitude of a bond length of D-pinitol follows  $C_1-C_2=C_1-C_6=C_2-C_3=1.53\text{Å}^0$ ,  $C_1-O_7=C_2-O_8=1.41\text{Å}^0$ ,  $C_3-C_4=C_4-C_5=C_5-C_6=1.52\text{Å}^0$ ,  $C_3-O_9=C_4-O_{10}=C_5-O_{11}=O_{12}-C_{13}=1.42\text{Å}^0$  and  $C_6-O_{12}= 1.43\text{Å}^0$  from the show results, it is clear that an excellent agreement with the experimental data. The hexagonal bond angle of the benzene ring of  $C_2-C_1-C_6=110.31\text{Å}^0$ ,  $C_2-C_1-O_7 = 109\text{Å}^0$ ,  $C_6-C_1-O_7=111\text{Å}^0$ ,  $C_2-C_3-O_9=106\text{Å}^0$ ,  $C_5-C_4-O_{10}=112\text{Å}^0$ ,  $C_4-C_5-O_{11}=107\text{Å}^0$ ,  $C_6-O_{12}-C_{13}=114\text{Å}^0$ from showing results, it is clear that an excellent agreement with that experimental data. The dissimilarity in bond angle may be observed due to the atoms which involve in bonding are presented **Fig 1**.

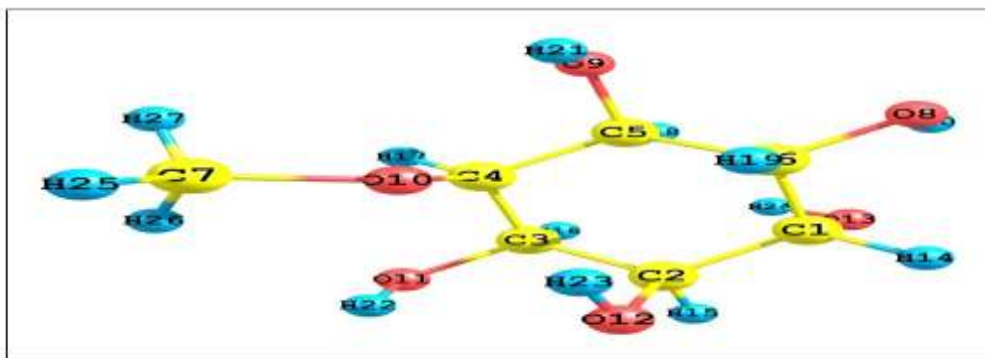


Fig.1 Optimized structure of D-pinitol

Table1. Optimized geometrical parameters like bond length and bond angles of D-Pinitol

Bond length	B3LYP/6-311++G(d,p)	Bond angle	B3LYP/6-311++G(d,p)
C <sub>1</sub> -C <sub>2</sub>	1.5308	C <sub>6</sub> -C <sub>1</sub> -O <sub>7</sub>	111.9114
C <sub>1</sub> -C <sub>6</sub>	1.5343	C <sub>1</sub> -C <sub>2</sub> -C <sub>3</sub>	109.5766
C <sub>1</sub> -O <sub>7</sub>	1.4168	C <sub>1</sub> -C <sub>2</sub> -O <sub>8</sub>	109.4778
C <sub>2</sub> -C <sub>3</sub>	1.5380	C <sub>3</sub> -C <sub>2</sub> -O <sub>8</sub>	109.7989
C <sub>2</sub> -O <sub>8</sub>	1.4198	C <sub>2</sub> -C <sub>3</sub> -C <sub>4</sub>	111.2568
C <sub>3</sub> -C <sub>4</sub>	1.5299	C <sub>2</sub> -C <sub>3</sub> -O <sub>9</sub>	106.8939
C <sub>3</sub> -O <sub>9</sub>	1.4236	C <sub>4</sub> -C <sub>3</sub> -O <sub>9</sub>	110.2086
C <sub>4</sub> -C <sub>5</sub>	1.5247	C <sub>3</sub> -C <sub>4</sub> -C <sub>5</sub>	111.3494
C <sub>4</sub> -O <sub>10</sub>	1.4237	C <sub>3</sub> -C <sub>4</sub> -O <sub>10</sub>	106.8448
C <sub>5</sub> -C <sub>6</sub>	1.5285	C <sub>5</sub> -C <sub>4</sub> -O <sub>10</sub>	112.1628
C <sub>5</sub> -O <sub>11</sub>	1.4238	C <sub>4</sub> -C <sub>5</sub> -C <sub>6</sub>	105.8109
C <sub>6</sub> -O <sub>12</sub>	1.4341	C <sub>4</sub> -C <sub>5</sub> -O <sub>11</sub>	107.8447
O <sub>12</sub> -C <sub>13</sub>	1.4241	C <sub>6</sub> -C <sub>5</sub> -O <sub>11</sub>	112.1075
<b>Bond angle</b>		C <sub>1</sub> -C <sub>6</sub> -C <sub>5</sub>	109.7651
		C <sub>2</sub> -C <sub>1</sub> -C <sub>6</sub>	110.3152
		C <sub>1</sub> -C <sub>6</sub> -O <sub>12</sub>	109.7217
		C <sub>6</sub> -O <sub>12</sub> -C <sub>13</sub>	114.1673

## 4.2 Vibration Assignments

The area of the vibrational analysis is to find vibrational assignments connected with specific molecular structures of a calculated compound. Entirely the vibrations are active in FT-IR and FT-Raman. The molecule has 27 atoms, hence, which possess 75 normal modes of vibrations. The B3LYP/6-311++G(d,p) calculated frequencies along with experimentally obtained FT-IR and FT-Raman spectral measurements are tabulated in **Table 2**. The observed and calculated frequencies using B3LYP/6-311++G(d,p) along with their relative, probable assignments and potential energy distribution (PED) of the title compound are condensed in **Table 2**. The maximum number of values determined by B3LYP/6-311++G(d,p) method are in good agreement with the experimental values. The observed and experimental FT-IR and FT-Raman spectra of D-pinitol are shown in the **Fig. 2 and 3** respectively.

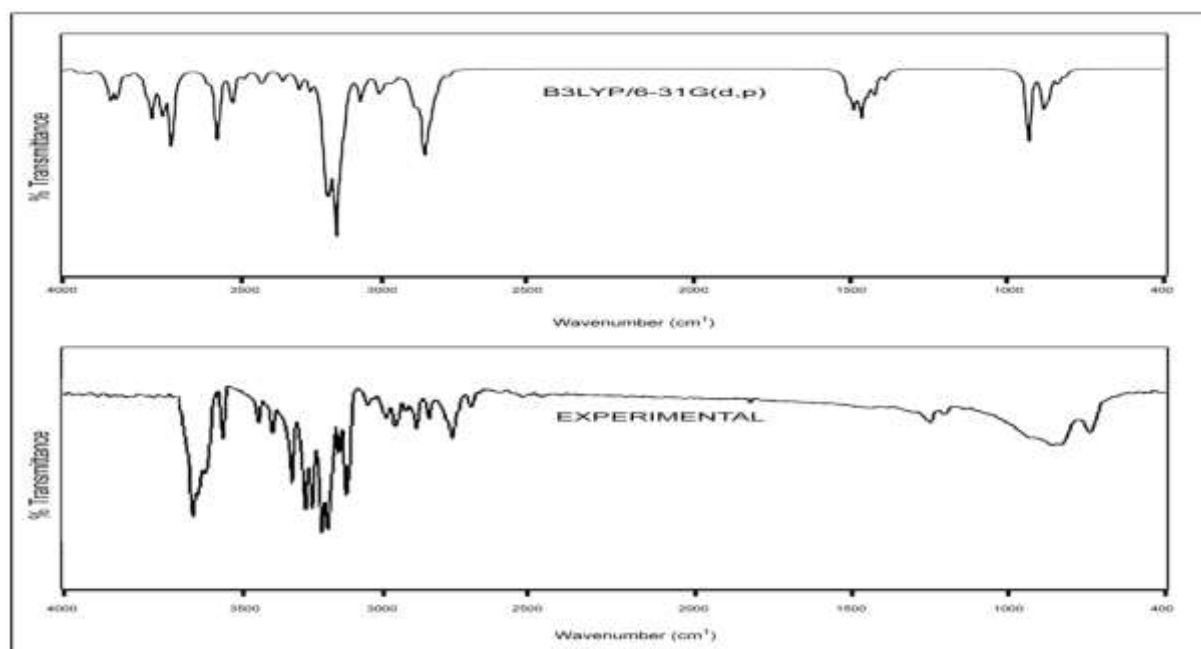


Fig.2 FT-IR spectrum of D-pinitol

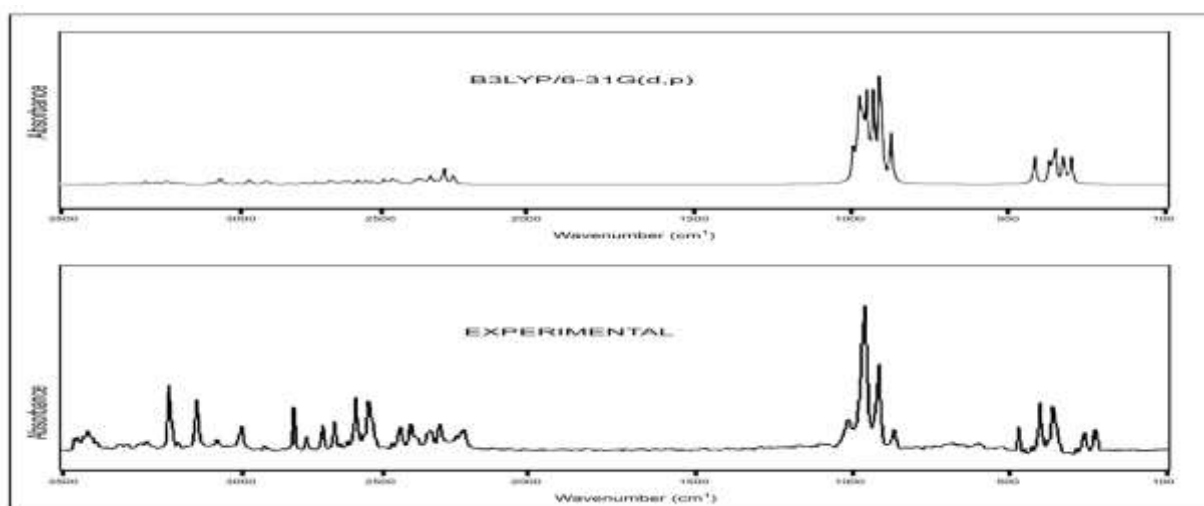


Fig. 3 FT-Raman spectrum of D-pinitol

### C-H Vibrations

The aromatic and hetero aromatic structures such as pyridine, pyrilium, thiapyrilium show C-H stretching vibrations act as fingerprint spectral region between  $3100 - 2900\text{cm}^{-1}$  [15,16]. In this spectral region, bands are not prominent noticeably by the nature of the functional groups experimentally in the title molecule of C-H vibration are observed at  $2998, 3040, 3055$  and  $3086\text{cm}^{-1}$  in FT-IR and  $3000, 3043, 3056$  and  $3075\text{cm}^{-1}$  in FT-Raman. The theoretical vibrations by B3LYP method also view clearly show good agreement with experimental. The vibration data involving C-H in-plane-bending in strongest absorptions for aromatic compounds occur in the spectral region  $1300-1000\text{cm}^{-1}$  and  $1000-650\text{cm}^{-1}$  due to the C-H out of plane bending [17-19] respectively and very useful for characterization purpose when there is in-plane interaction above  $1200\text{cm}^{-1}$ . C-H usually move in opposite direction [17]. For our title molecule, the C-H in-plane bending vibration is found at  $1020$  and  $1206\text{cm}^{-1}$  in FT-IR and at  $1026$  and  $1203\text{cm}^{-1}$  in FT-Raman. The theoretical calculation vibrations by B3LYP method also show good agreement with experimental data. The out-of-plane bending spectral vibration is observed at  $656, 748, 775$  and  $823\text{cm}^{-1}$  in FT-IR, and at  $639, 753, 780$  and  $837\text{cm}^{-1}$  in FT-Raman. This theoretical calculation vibration in B3LYP/6-311++G(d,p) method also show good agreement with experimental data, with these vibrational modes, are also confirmed by their PED values.

### C-C Vibrations

The ring C-C stretching vibration is very important in the spectrum and highly characteristic vibrations stretching give rise to a characteristic peak in the spectral region of 1600-1000  $\text{cm}^{-1}$  and are not significantly influenced by the nature of the replacement about the ring[20]. In the present study C-C stretching vibrations are observed at 1020,1070,1080,1013, 1126 1159,1242,1306,1378,1410, and 1426  $\text{cm}^{-1}$  in FT-IR spectrum and FT-Raman bands were observed at 1026,1082,1113,1126,1162,1301,1381,1412 and 1427  $\text{cm}^{-1}$ . The theoretical values calculated were obtained in the range 1023 to 1421  $\text{cm}^{-1}$  by B3LYP/6-311++G(d,p) method and shows clearly that the theoretical values are in very good agreement with experimental values in give **Table 2**.

### C-O Vibrating

The title compound method methoxy group in aromatic ring includes C-O band, where two different types of carbon are calculated are attached to oxygen and visible in two different regions C-O vibration is with high sensitivity and strong intensity of absorption to moderately minor changes in its environment. Intra and intermolecular factors affected C-O absorptions inorganic compounds due to inductive, field effects, conjugation effects and mesmeric effects[21]. The C-O stretching vibration occurs with strong band spectral region 1000-1230[22]. In the title compound C-O vibrations are observed of which 1070,1082,1113,1126,1159, 1187 and 1206  $\text{cm}^{-1}$  in FT-IR and at 1082, 1111, 1126,1162,1191,and 1203  $\text{cm}^{-1}$  in FT-Raman showing excellent dependability with theoretical values at 1076, 1085,1117,1121,1160,1111 and 1207  $\text{cm}^{-1}$  B3LYP/6-311++ method. In title compound of in-plane and out-plane, the vibration generally occurs in 670 to 330  $\text{cm}^{-1}$  [23-27]. In the present molecule 332,356,414,444,472,501 in FT-IR and FT-Raman 329,352,394, 419,438,468,479,511 and 528 in both spectra in meantime, theoretical values are slightly levels than the expected, while, experimental values agree with spectral data recorded in literature.

### CH<sub>3</sub> Vibrations

The title of molecules D-Pinitol, possess a CH<sub>3</sub> group in the hetro aromatic ring shown in **Fig 2 and 3**. For the vibration assignment of CH<sub>3</sub> group one can expect nine fundamentals, namely CH<sub>3</sub>ss – symmetric stretch, CH<sub>3</sub>Sb-symmetric bending, CH<sub>3</sub> ips–in-plane stretch (in-plane hydrogen stretching mode); CH<sub>3</sub>ipb –in-plane bending (i.e-in-plane hydrogen deformation mode); CH<sub>3</sub> t –twisting mode, CH<sub>3</sub>opb – out-of-plane bending modes, CH<sub>3</sub>ipr – in-plane rocking, CH<sub>3</sub> – opr- out-of-plane rocking. The C-H vibration stretching in methyl occurs at lower frequencies than those of aromatic ring (3000-3100  $\text{cm}^{-1}$ )[28,29] and in the present study, the vibration mode observed at 3022  $\text{cm}^{-1}$  in the FT-IR spectrum at 3019  $\text{cm}^{-1}$  in FT-Raman spectrum and 3027  $\text{cm}^{-1}$  theoretically are vibration assigned. The asymmetric bending vibrations mode of CH<sub>3</sub> group typically appear in the spectral region 1465-1440  $\text{cm}^{-1}$  and 1390-1370  $\text{cm}^{-1}$  [30,31]. In this study, the calculated asymmetric bending vibrations of CH<sub>3</sub> obtained at 1465, in FT-IR and 1470 in FT-Raman respectively the experiment symmetric bonding of CH<sub>3</sub> vibration were 7 modes of CH<sub>3</sub> observed at 166  $\text{cm}^{-1}$  by the DFT/6-311++ calculation and 155  $\text{cm}^{-1}$  in FT-Raman which coincides very most with calculated and literature [32,33].

### O-H Vibrations

The O-H functional group there are three vibrations stretching in-plane bending and out-of-plane bending bands due to O-H stretching vibration medium to strong intensity in FT-IR spectrum band is generally weak in FT-Raman spectrum[34]. The O-H –in-plane, and O-H out of plane bending vibration is observed 1440-1260  $\text{cm}^{-1}$  and 875-960  $\text{cm}^{-1}$  [35]. The O-H groups strongly in the spectral region 3700-3400  $\text{cm}^{-1}$  [36,37]. In D-Pinitol, the O-H stretching vibration. Observed at 3543,3596,3606, 3617,3623 in FT-IR at 3537 as very most, 3586,3608,3613 and 3622 FT-Raman spectra. The theoretical values 3538,3594, 3600,3616 and 3619 are also O-H stretching of D-Pinitol vibrational by B3LYP/6-311++G(d,p). The O-H in-plane bending spectral vibration as the very most band at 1338,1378,1410, 1426 in the FT-IR spectrum and 1338,1350,1381,1412 in the FT-Raman spectra. The O-H out of plane bending spectral vibrations observed at 915 in FT-IR, at 922 FT-Raman. The theoretical values 921 are also assigned to O-H out of plane bending by B3LYP/6-311++G(d,p), **Table 2**.

Table 2 Vibrational assignments of D-Pinitol

Experimental		Calculated	Vibrational Assignments+PED (%)
FT-IR cm <sup>-1</sup>	FT-R cm <sup>-1</sup>	B3LYP/6- 311++G(d,p) $\nu$ cm <sup>-1</sup>	
-	80	83	$\tau$ HCOC(47)
-	103	98	$\tau$ COCC(38) + $\tau$ CCCC(31)
-	116	118	$\tau$ COCC(53) + $\tau$ CCCC(12)
-	155	166	$\delta$ OCC(54) + $\tau$ CH <sub>3</sub> (57)
-	185	171	$\delta$ OCC(21) + $\tau$ HCOC(37)
-	204	200	$\delta$ OCC(13) + $\gamma$ OCCC(24)
-	215	222	$\delta$ OCH(45)
-	259	261	$\delta$ OCC(50)
-	263	269	$\delta$ OCC(50)
-	-	276	$\delta$ OCC(50)
-	289	287	$\delta$ OCC(54) + $\tau$ HCOC(36)
-	314	310	$\delta$ OCC(59)
-	332	329	$\delta$ OCC(27)
-	356	352	$\delta$ COC(54) + $\tau$ HCOC(10)
-	381	394	$\gamma$ COCC(30)
-	414	419	$\delta$ OCC(20) + $\tau$ HOCC(22)
-	444	438	$\tau$ HOCC(39)
-	472	468	$\tau$ HOCC(79) + $\gamma$ OCCC(10)
-	465	479	$\tau$ HCCO(69)
-	501	511	$\tau$ HOCC(76)
-	-	528	$\delta$ OCC(10) + $\tau$ OCCC(10)
656	639	642	$\delta$ CCH(35)
674	669	669	$\gamma$ OCCC(11)
694	694	680	$\tau$ HOCC(79)
748	753	736	$\gamma$ CCCH(31)
775	780	780	$\gamma$ CCCH(37)
823	837	838	$\delta$ CCH(12) + $\gamma$ CCCH(11)
857	856	849	$\gamma$ CCOC(17)
915	922	921	$\delta$ CCH(58)
975	978	981	$\gamma$ CCCH(28)
1020	1026	1023	$\gamma$ CCCH(22)
1055	1052	1061	$\delta$ CH <sub>2</sub> (37)
1070	1082	1076	$\nu$ OC(46) + $\gamma$ OCCC(16)
1082	-	1085	$\gamma$ OCCC(42)
-	-	1097	$\nu$ OC(42) + $\gamma$ OCCC(36)
1013	1111	1117	$\nu$ OC(27) + $\gamma$ OCCC(46)
1126	1126	1121	$\gamma$ OCCC(38)
-	-	1134	$\gamma$ OCC(40)
1159	1162	1160	$\nu$ OC(32) + $\gamma$ OCC(22)
1187	1191	1181	$\tau$ CH <sub>3</sub> (35)
1206	1203	1207	$\delta$ HCH(10) + $\tau$ CH <sub>3</sub> (29)

-	-	1213	$\delta$ HOC(14)
1239	1241	1234	$\nu$ OC(39)+ $\delta$ HOC(23)
1242	-	1257	$\gamma$ CCCH(12)
1275	1277	1277	$\gamma$ CH <sub>3</sub> (21)
-	-	1293	$\nu$ OC(42)+ $\tau$ HCCO(20)
1306	1301	1308	$\gamma$ CCCH(11)
-	-	1321	$\delta$ HOC(12)
1338	1338	1334	$\delta$ OCH(35)
-	1350	1362	$\delta$ HCO(11)
1378	1381	1383	$\delta$ HCO(15)+ $\gamma$ CCCH(17)
-	-	1399	$\delta$ HCO(40)
1410	1412	1408	$\delta$ HCO(11)+ $\gamma$ CCCH(14)
1426	1427	1421	$\nu$ CC(33)+ $\delta$ HOC(10)+ $\delta$ HCO(28) + $\gamma$ CCCH(16)
-	1442	1440	$\delta$ HOC(53)+ $\nu$ CH(31)
1449	-	1447	$\delta$ HOC(35)+ $\delta$ HCO(14)+ $\gamma$ CCCH(12)
-	1457	1451	$\nu$ CH(42)+ $\delta$ HOC(54)
1465	1470	1469	$\delta$ HOC(48)+ $\gamma$ CH <sub>3</sub> (32)
-	1491	1489	$\delta$ CH <sub>3</sub> (46)+ $\delta$ HOC(18)
1501	-	1499	$\delta$ CH <sub>3</sub> (72)
1531	1532	1532	$\delta$ HCH(54)
2998	3000	3002	$\nu$ CH(4)
3022	3019	3027	$\nu$ CH <sub>3</sub> (89)
3040	3043	3038	$\nu$ CH(86)
3055	3056	3054	$\nu$ CH(94)
-	-	3059	$\nu$ CH(91)
3086	3075	3080	$\nu$ CH(93)
-	-	3104	$\nu$ CH(94)
3111	-	3108	$\nu$ CH(97)
3139	-	3146	$\nu$ CH(99)
3543	3537	3538	$\nu$ OH(88)
3596	3586	3594	$\nu$ OH(98)
3606	3608	3610	$\nu$ OH(100)
3617	3613	3616	$\nu$ OH(100)
3623	3622	3619	$\nu$ OH(100)

$\nu$ -stretching; $\delta$ -in-plane-bending; $\tau$ -torsion; $\gamma$ -out-of-plane-bending

### 4.3 Natural Bond Orbital

Natural bond analysis has been achieved extensive usage in dynamic behaviors of community and electronic structure system [38,39]. The NBO analysis is an efficient method to investigate the intra and intermolecular interactions and charge transfer or conjugative from the filled (Bonding or lone pair) to virtual orbital spaces (antibonding and Rydberg)[40]. The NBO procedure uses mainly information pertaining to the atomic orbital over the lab and density matrices. The natural atomic orbitals (NAOs) transformation to the orthogonalization which is followed by a bond orbital transformation to get the NBOs[41]

### Second Order Perturbation Analysis

The NBO analysis carried out second-order perturbation theory helps to detect the role of all possible interaction between filled donor Lewi's type NBOs and estimating they are energetic. The occupied and unoccupied NBO undergo a delocalization of electron density corresponding to an electron donor to electron

can of acceptors interaction and have the degree of conjugation of the system is measured by the hyper conjugative interaction energy  $E(2)$  [41]. NBO calculations were performed using Gaussian NBO version. For each donor (i) and acceptor (j), the stabilization energy associated with  $i \rightarrow j$  delocalization.

$$E_2 = -n_0 \frac{\langle \sigma | F | \sigma \rangle}{\epsilon_{\sigma^*} - \epsilon_{\sigma}} = -n\sigma \frac{F^2_{ij}}{\Delta E}$$

NBO results presented in **Table 3**, are significant in order to conclude whether some variation of ions increase or decrease the electrostatic nature of interaction from the **Table 3**. In D-pinitol interaction between the first lone pair of  $O_{10}$  and antibonding of  $\sigma^* O_{12}-H_{23}$  has the highest  $E(2)$  value around 11.05 Kcal/Mol. The other important interaction giving stronger stabilization energy value of 8.43 Kcal/Mol to antibonding  $\sigma^* C_{12}-C_6$  between the lone pair of oxygen  $O_8$  and occupancy of electrons and P-character. The natural localized molecular orbital (NLMO) study has been carried out since they expression how bonding in a molecule is composed of orbitals localized on different atoms. The origin of NLMOs from NBOs gives direct insight into the nature of the localized molecular orbital's "delocalization tails" [42,43]. **Table 3**, shows significant NLMO's occupancy, the percentage of parent NBO and atomic hybrid contributions of D-pinitol calculated at the B3LYP level using 6-31++G(d, p) basis set. The NLMO of a second lone pair of Oxygen atom  $O_{10}$  is the most delocalized NLMO and has only 96% contribution from the localized LP(2)  $O_{10}$  parent NBO, and the delocalization tail (~3%) consists of the hybrids of  $O_{12}$  and  $H_{23}$ .

**Table 3 NBO/NLMO analysis of D-Pinitol**

Donor	Acceptor	E(2)Kj/Mol	Hybrid	ED(e)	%From Parent Nbo	Hybrid Atom	Cont Atom	Atom	Percentage
LP(2) $O_8$	$\sigma^* C_5-C_6$	8.34	$P^{1.00}$	1.95342	97.647	$C_5, C_6$	1.973	$O_8$	99.98
LP(2) $O_9$	$\sigma^* C_4-C_5$	6.62	$P^{1.00}$	1.95577	97.769	$C_4, C_6$	1.587	$O_9$	99.99
LP(2) $O_{10}$	$\sigma^* O_{12}-H_{23}$	11.05	$P^{1.00}$	1.92942	96.458	$O_{12}, H_{23}$	3.220	$O_{10}$	99.99
LP(2) $O_{11}$	$\sigma^* C_3-C_4$	7.71	$P^{1.00}$	1.95391	97.678	$C_3, C_4$	1.606	$O_{11}$	99.99
LP(2) $O_{12}$	$\sigma^* C_1-C_2$	6.93	$P^{1.00}$	1.93934	96.949	$C_1, C_2$	2.862	$O_{12}$	99.99
LP(2) $O_{13}$	$\sigma^* C_1-C_6$	4.70	$P^{1.00}$	1.95350	97.660	$C_1, C_6$	1.949	$O_{13}$	99.99

#### 4.4 Molecule Electrostatic Potential

The molecule electrostatic potential (MEP) at a point in force acting on a proton located in the space around a molecule given an electrical charge clouded generated, electron and nuclei provide [44]. The molecular electrostatic potential (MEP) surface map is plotted over the optimized structure of D-Pinitol in order to investigate the polarity of the charged molecule and mapping an electron density isosurface with electrostatic potential surface, shape, size negative, the positive and physico-chemical reactivity of mentioned molecules. It is recognized as a supportive parameter which characterizes [45,46]. In different values of the MEP, at the surface are represented by different colors, the maximum negative region represents the site for electrophilic attack indicated by red colors while the maximum positive region represents nucleophilic attacked in indicated region represents green. The 3D diagram of MEP for the D-Pinitol compound at B3LYP/6-311++G(d,p) basis set is shown in **Fig 4**, the color codes region represented maps are in the range from -0.0409 au (deepest red) to 0.05000 au (deepest blue) for D-pinitol respectively.

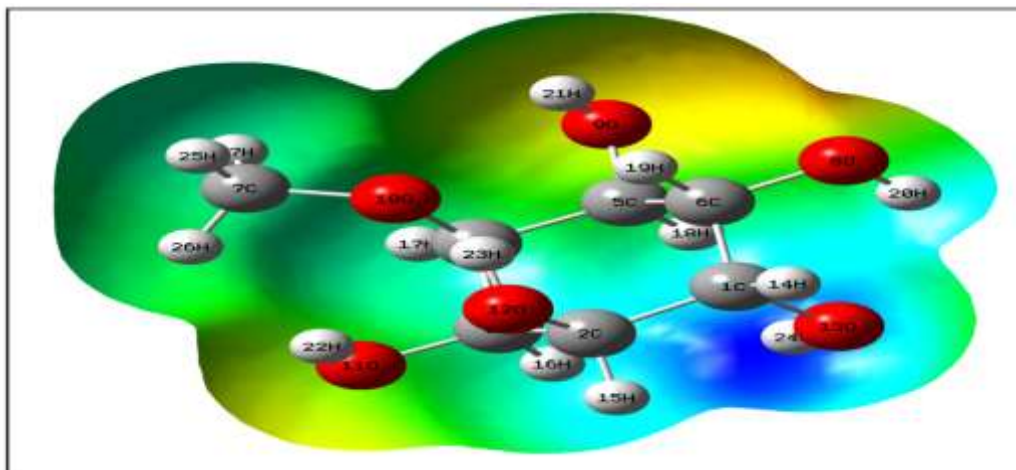


Fig.4 Molecular electrostatic potential of D-pinitol

#### 4.5 Molecular Transport Properties

Molecular orbital theory approaches, the energy gap between HOMO-LUMO is an important in chemical reactivity of the molecules such as hardness, softness, electronegativity and electrophilicity index as well as all local reactivity and formative molecular electrical transport properties, of kinetic stability, optical polarizability[47-51] are shown in **Fig 5**. The highest occupied molecular orbitals (HOMOs) and lowest lying unoccupied molecular orbitals (LUMOs) are named as frontier molecular orbital (FMOs). The quantum bonding features of D-Pinitolis depicted by a plot of the HOMO-LUMO. Progress, the parameters

like Hardness ( $\eta$ ), the chemical potential ( $\mu$ ) and electronegativity ( $\chi$ ) and softness (S), electrophilicity index ( $\omega$ ) were well-defined using the above mentioned energy values. Which are defined follow.

$$\eta = \frac{1}{2} \left( \frac{\partial^2 E}{\partial N^2} \right) V(r) = \frac{1}{2} \left( \frac{\partial \mu}{\partial N} \right) V(r)$$

$$\mu = \left( \frac{\partial E}{\partial N} \right) V(r)$$

$$\chi = -\mu = - \left( \frac{\partial E}{\partial N} \right) V(r)$$

$$S = \frac{1}{\eta}, \eta = \frac{I-A}{2}, \mu = \frac{-(I+A)}{2}, \chi = \frac{I+A}{2}, \omega = \frac{\mu^2}{2}$$

Using the above equations, the chemical potential, hardness, and electrophilicity index, electronegativity and softness are being calculated for D-Pinitol and their values as shown in **Table 4**. The functionality of this new reactivity quantity has been recently demonstrated in mastery the toxicity of various pollutants in terms of their reactivity and site selectivity [52-54].

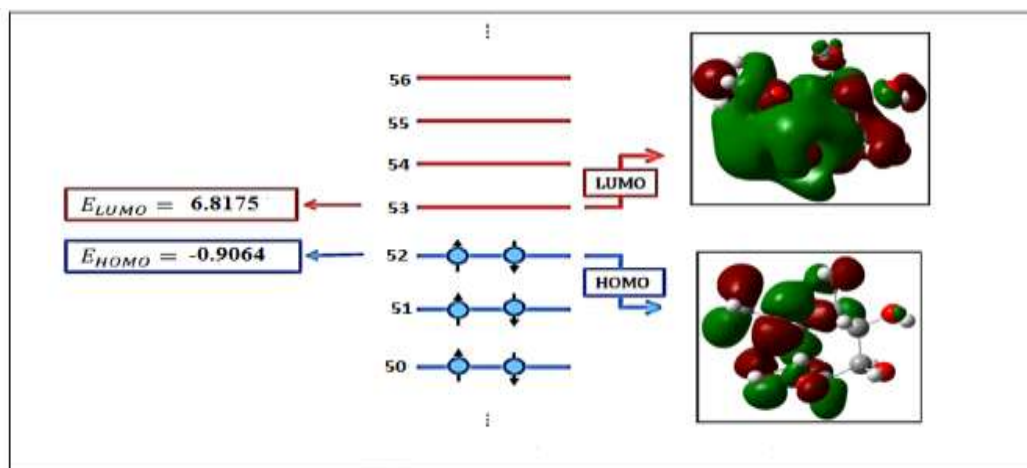


Fig. 5 Frontier molecular orbital of D-pinitol

Table 4 Molecular properties of D-Pinitol

Molecular properties	B3LYP\6-31G(d,p)	Molecular properties	B3LYP\6-31G(d,p)
$E_{HOMO}(eV)$	6.8175	Chemical Hardness( $\eta$ )	7.2708
$E_{LUMO}(eV)$	-0.9064	Softness(S)	0.1375
$E_{Homo-Lumo}gap(eV)$	7.7240	Chemical Potential( $\mu$ )	-6.3643
Ionisation	-6.8175	Electronegativity( $\chi$ )	6.36438
Electron affinity (A)	0.9064	Electrophilicity	20.2526

#### 4.6 Molecular Docking Studies of (compound name) Against Myeloperoxidase

Oxidative stress is mostly associated with inflammation. This is particularly dominated by neutrophils, which has a huge capacity to generate reactive oxygen species (55-57). It uses hydrogen peroxide to catalyze the production of hypohalous acids as well as an excess of free radicals (58). These reactive intermediates readily oxidize lipids, proteins, and DNA (59,60). Hypochlorous acid and hypobromous acid are kinetically the most reactive two-electron oxidants produced *in vivo* (60). Hypochlorous acid is a potent toxin, and at low levels, it activates stress response pathways within cells (62). Identification of specific biomarkers of hypochlorous acid at sites of inflammation has confirmed that MPO contributes to protein damage in cystic fibrosis (63), atherosclerosis (64), and atrial fibrillation (65). The convincing evidence that MPO produces damaging oxidants at sites of inflammation has focused attention on it as a pharmacological target. Currently, there is no effective inhibitor of the enzyme and limited appreciation of the best routes to block its activity. The present study is to find the better inhibitor for this enzyme.

The  $O_2$  atom of the hydroxyl group of the co-crystal ligand **Fig 6** interacts with the  $N_2$  atom of the amide group of PHE147 at a distance of 3.0 Å. It also interacts with the  $O_2$  atom of the GLU 102 at a distance of 2.5 Å with the glide score of -5.14 and glide energy of - 26.22 kcal/mol.

In the (D-Pinitol) the three hydroxyl group interacts with the  $N_2$  atom of amide group of the ARG 124,  $N_2$  atom of amide group of PHE 147 and with the  $O_2$  atom of GLU 102 at a distance of 3.0Å, 3.0Å, 3.0Å, 2.5Å and 2.8Å, respectively. The docking results obtained the glide score of -5.29 and glide energy of - 26.59 kcal/molis shown in **Table 5**. The D-Pinitol shows the good H-bond interaction, glide score and glide energy than the existing co-crystal ligand is shown in the **Fig.6 & 7**. It may act as an inhibitor of the inflammation disease.

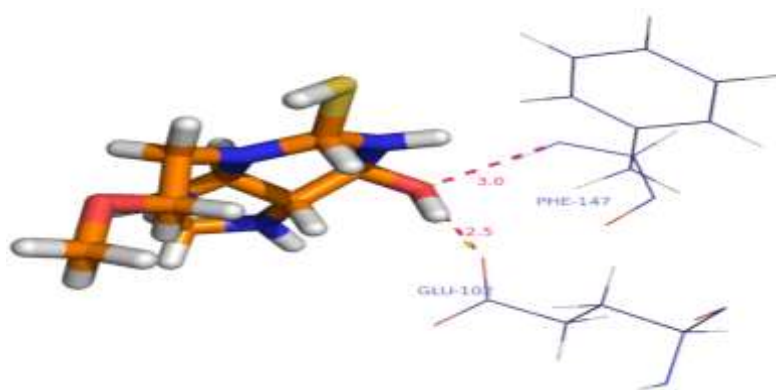


Fig. 6PVW (Co-crystal) of D-pinitol

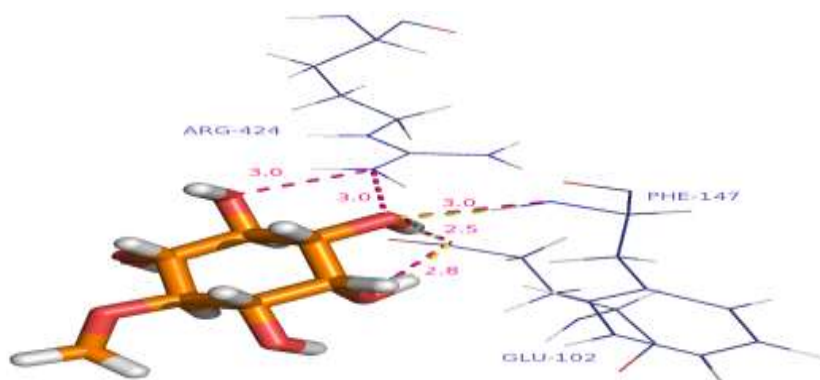


Fig. 7 Molecular docked model of o of D-pinitol

Table 5 Molecular Docking Studies Of (D-Pinitol) Against Myeloperoxidase

Compounds	H-bond interactions D-H...A	Distance (Å)	Glide score	Glide energy (kcal/mol)
(PVW) Co-crystal	(PHE 147)N-H...O O-H...O(GLU 102)	3.0 2.5	-5.14	-26.22
Compound name	(ARG424)N-H...O (ARG 424)N-H...O (PHE 147)N-H...O O-H...O(GLU 102) O-H...O(GLU 102)	3.0 3.0 3.0 2.5 2.8	-5.29	-26.59

#### 4.7 UV Analysis

To understand nature of electronic transitions of D-Pinitol molecule has been recorded within 200-800 nm for discovered in methanol solvent **fig 8**. The obtained UV radiation was electronic absorption wavelength by molecules passes from a state of the ground to the excited state. There are one excitation transitions of UV-Visible spectra of D-Pinitol. These bands are reported at 239 nm and electronic transitions of the title molecule of D-Pinitol was studied using time-dependent DFT (TD-DFT) calculation 239 nm in the methanol solvent was theoretically analysis using in present **Table 6**. Electronic transition from HOMO->LUMO (96%), HOMO->L+1 (56%) and H-1->LUMO (63%), HOMO->L+1 (31%) with contribution. The observed transition from HOMO->LUMO is  $n \rightarrow \pi^*$ .

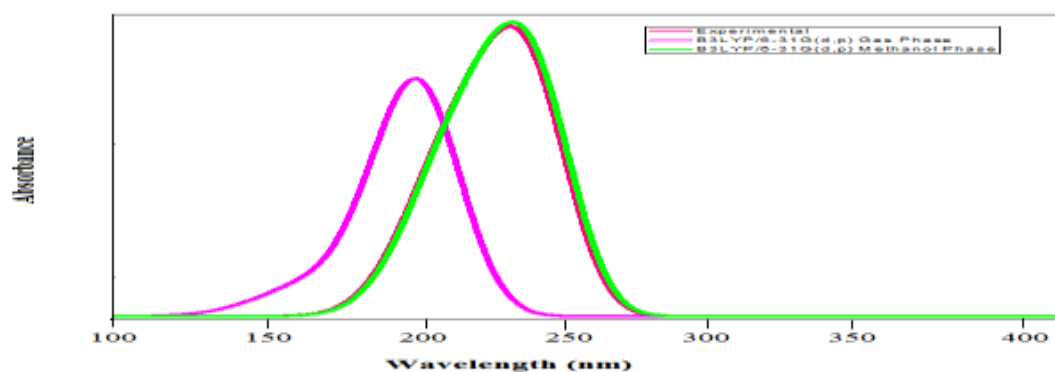


Fig.8 UV-Spectrum of D-pinitol

Table 6 The UV-vis excitation energy of D-Pinitol

States	TD-B3LYP/6-31G(d,p)		Expt. $\lambda_{obs}$	Major Contributions
	Methanol			
	$\lambda_{cal}$	E(eV)		
S1	241.09	7.2466	239	HOMO->LUMO (96%)
S2	216.20	7.4601	214	HOMO->L+1 (56%)
S3	212.43	7.6333	213	H-1->LUMO (63%), HOMO->L+1(31%)

#### 4.8 Conclusion

The prophesied structural of the D-Pinitol were investigated thoroughly and analyzed using high-level quantum chemistry calculation. The optimized geometrical parameters and vibrational frequencies FT-IR, FT-Raman calculated of the fundamental modes of D-Pinitol have been obtained from DFT/B3LYP/6-311++G(d,p). Experimentally observed frequencies assignment is in very good agreement with quantum chemical theoretical calculation. The NBO analysis conforms, the interaction energy formed by the orbital overlaps  $LP_{(2)} O_{10}$  and  $\sigma^* O_{12}-H_{23}$  and  $E_{(2)} = 11.05$  Kal/molan actual close to pure P-type lone pair orbital participates in the electron donation to the  $LP_{(2)} O_8$  accept  $\sigma^* C_5-C_6$  and  $E_{(2)} = 8.34$  Kal/mol. The MEPs and electron densities of D-Pinitol lie in the range from -0.0409 au (deepest red) to 0.0500 au (deepest blue) respectively for D-Pinitol. Finally, HOMO-LUMO energy gap discloses that charge transfer occurs in the molecules, which are responsible for the bioactive property of the biomedical compound D-Pinitol.

#### References

1. Croze M.L., Vella R.E., Pillon N.J., Soula H.A., Hadji L., Guichardant M., and Soulage C.O., J.Nutri. Biochem. 2013, 24, 457-466.
2. Agarie S., Kawaguchi A., Kodera A., Sunagawa H., Kojima H., and Nose A., et al., Plant Prod Sci 2009, 12, 37-46.
3. Talbot Jr., Seidler R.J. Cyclitol utilization associated with the presence of AKlebsiellae in botanical environments. Appl. Environ. Microb. 1979, 37, 909-15.
4. Bates S.H., Jones R.B., Bailey C.J. Insulin-like effect of pinitol. Brit. J. Pharmacol. 2000, 130, 1944-8.
5. Singh R.K., Pandey B.L., Tripathi M., Pandey V.B. Anti-inflammatory effect of (+)-pinitol. Fitoterapia. 2001, 72, 168-70.
6. Lin T.H., Tan T.W., Tsai T.H., Chen C.C., Hsieh T.F., Lee S.S., et al., Int J Mol Sci 2013, 14, 9790-802.
7. Paul M.J., Cockburn W., J. Exp. Bot. 1989. 40, 1093-1098.
8. Gomes C.I, Obendorfa R.L., Horbowicz bM. Crop Sci. 2005, 45, 1312-1319.
9. Kim J.I., Kim J.C., Kang M.J., Lee M.S., Kim J.J., Cha I.J., Eur. J. Clin. Nutr. 2005, 59, 456-458.
10. Geethan P.K., Prince P.S., J. Biochem. Mol. Toxicol. 2008, 22, 220-224.

11. Frisch H.J, Trucks G.W, Schlegel H.B, Scuseria G.E, Robb M.A, Cheeseman J.R, Nakatsuji H, Caricato M, Li X, Hratchian H.P, Toyota K, Fukuda R, Hasegawa J, Ishida M, Nakajima R, Honda Y, Kitao O, Nakai H, Vreven T, Montgomery Jr J.A., Peralta J.E., Ogliaro F., Bearpark M., Heyd J.J., Brothers E., Kudin K.N., Staroverov V.N., Kobayashi R., Normand J., Ragavachari K., Rendell A., Burant J.C., Tomasi S.J., Cossi M., Rega N, Millam J.M, Klene M, Knox J.E, Cross J.B, Bakken V, Adamo C, Jaramillo J, Gomperts R., Stratmann R.E., Yazyev O, Austin A.J, Cammi R, Ochterski J.W, Martin R.L, Morokuma K, Zakrzewski V.G, Voth G.A, Salvador P, Dannenberg J.J, Dapprich S, Daniels A.D, Farkas O, Foresman J.B, Gaussian O.G., Revision A.02, Gaussian Inc., Willingford, CT, 2009.
12. Jamroz M.H., Vibrational energy distribution analysis: VEDA 4 Program Warsaw, Poland, 2004.
13. Frisch E., Hratchian H.P., Dennington I.R., Keith T.A., John Millam, Nielsen A.B., Holder A.J., Hincok J. Gaussian, Inc., GaussView Version 5.0., 2009.
14. Dowd M.K., Stevens E.D. - Taylor & Francis. Journal of carbohydrate chemistry. 2002;21, 373–383.
15. Varsányi G., Assignments for Vibrational Spectra of Seven Hundred Benzene Derivatives, Halsted Press, 1974.
16. Govindarajan M., Ganasan K., Periandy S., Karabacak M., Mohan S., Spectrochim. Acta A, 2010, 77, 1005–1013.
17. Sato H., Dybal J., Murakami R., Noda I., Ozaki Y., J. Mol. Struct. 2005, 744–747, 35–46.
18. Rajesh P., Gunasekaran S., Gnanasambandan T., Seshadri S., Spectrochim Acta Part A. 2016, 153, 496–504.
19. Bardak F., Karaca C., Bilgili S., Atac A., Mavis T., Asiri C.A.M., Karabacak M., Kose E., Spectrochim Acta Part A. 2016, 165, 33–46.
20. Singh H., Singh S., Srivastava A., Tandon P., Bharti P., Kumar S., Dev K., Maurya R., J. Mol. Struct. 2016.10.077.
21. Varsanyi G., Vibrational Spectra of Benzene Derivatives, Academic Press, New York, 1969.
22. Koczon P., Lewandowski W., Mazurek A.P., Vib. Spectrosc. 1999, 20, 143–149.
23. Sundaraganesan N., Kumar K.S., Meganathan C., Joshua B.D., Spectrochim. Acta A 2006, 65, 1186–1196.
24. Lakshmaiah B., Rao G.R., J. Raman Spectrosc. (1989) 20, 439–448.
25. Reddy B.V., Rao G.R., Vib. Spectrosc. 1994, 6, 231–250.
26. Campagnaro G.E., Wood J.L., J. Mol. Struct. 1970, 6 (2), 117–132.
27. Hakan Arslan, Oztekin Algul, Int. J. Mol. Sci. 2007, 8, 760–776.
28. Roeges N.P.G., A Guide to the Complete Interpretation of IR Spectra of Organic Compounds, Wiley, New York, 1994.
29. Bunce S.J., Edwards H.G., Johnson A.F., Lewis I.R., Turner P.H., Spectrochim. Acta. 1993, 49, 775.
30. Colthup N.B., Daly, Wiberly S.E. Introduction to IR and Raman Spectroscopy, Academic Press, New York, 1990.
31. Socrates G., Infrared Characteristic Group Frequencies, Wiley–Interscience Publication, New York, 1990.
32. Joseph L., Sajan D., Shettigar V., Chaitanya K., Misra N., Sundius T., Nemecl, Mater. Chem. Phys. 2013, 141, 248.
33. Tarchounan S., Chaabane I., Ben Rahaiem A., Physica E. 2016, 83, 186–194.
34. Koczon P., Lewandowski W., Mazurek A.P., Vib. Spectrosc. 1999, 20, 143–154.
35. Socrates G., Infrared and Raman characteristics Group frequencies, 3rd edition, Wiley, New York, USA, 2001.
36. Karabacak M., Kose E., Atac A., Spectrochim. Acta. 2012, 91A, 83–96.
37. I.D. Sadekov Russ. Chem. Rev. 1970, 30, 179–195.
38. Weinhold F., In Encyclopedia of Computational Chemistry, Schleyer P. v. R., Allinger N. L., Clark T., Gasteiger J., Kollman P. A., Schaefer H. F., III, Schreiner P. R., Eds.; Wiley: Chichester, UK, 1998, 3, 1792–1811;
39. For a bibliography of recent NBO applications, see <http://nbo6.chem.wisc.edu/biblio.htm>. Accessed Feb. 1, 2013.
40. For a current list of NBO-affiliated and NBO6-compatible programs, see <http://nbo6.chem.wisc.edu/affil.htm>. Accessed Feb. 1, 2013.
41. Esme, A.; Sagdinc, S.G. The Vibrational Studies and Theoretical Investigation of Structure, Electronic and Non-linear Optical Properties of Sudan III [1-{{4- (phenylazo) phenyl} azo}-2-naphthalenol], J. Mol. Struct. 2013, 1048, 185–195.

42. Reed, A.E.Weinhold, F.; Curtiss, L.A.; Pochatko, D.J. Natural Bond Orbital Analysis of Molecular Interactions: Theoretical Studies of Binary Complexes of HF, H<sub>2</sub>O, NH<sub>3</sub>, N<sub>2</sub>, O<sub>2</sub>, F<sub>2</sub>, CO, and CO<sub>2</sub> with HF, H<sub>2</sub>O, and NH<sub>3</sub>, *J. Chem. Phys.* 1986, 84, 5687–5705.
43. Reed A. E., Schleye P. V. R. *Inorg Chem.* 1988, 27, 3969–3987.
44. Xavier R. J., Gobinath E. *Spectrochim. Acta A.* 2012, 91, 248–255.
45. Sakthivel S., Alagesan T., Muthu S., Abraham C. S., Geetha E., *Journal of Molecular Structure* ,2017, S0022-2860 ,31644-7.
46. Silverstein R. M., Bassler G. C. and Morill T. C. , *Spectrometric Identification of Organic Compounds*, 4th ed. Wiley, 1981.
47. Parr R. G., Szentpaly L., Liu S., *J. Am. Chem. Soc.* 1999, 121, 1922–1924.
48. Chattaraj P K, Maiti B, Sarkar U. *J Phys Chem.* 2003, 107: 4973–4975.
49. Parr R. G., Donnelly R. A., Levy M., Palke W. E. *J Chem Phys.* 1978, 68, 3801–3807.
50. Parr R. G., Pearson R. G. *J. Am. Chem. Soc.* 1983, 105, 7512–7516.
51. Parr R. G., Chattaraj P. K. *J. Am. Chem. Soc.* 1991, 113, 1854–1855.
52. Parthasarathi R., Padmanabhan J., Elango M., Subramanian V., Chattaraj P. *Chem Phys Lett.* 2004, 394, 225–230.
53. Parthasarathi R., Padmanabhan J., Subramanian V., Maiti B., Chattaraj P. *Curr Sci* 2004, 86, 535–542.
54. Parthasarathi R., Padmanabhan J., Subramanian V., Sarkar U., Maiti B., Chattaraj P. *J Mol Des.* 2003, 2, 798–813.
55. Klebanoff S. J., in *Inflammation: Basic Principles and Clinical Correlates* 1999, 721–768.
56. Nicholls S. J., Hazen S., *Arterioscler Thromb Vasc Biol.* 2005, 25, 1102–1111.
57. Davies M. J., Hawkins C. L., Pattison D. I., Rees M. D. *Antioxid Redox Signal*, 2008, 10 1199–1234.
58. Kettle A. J., Winterbourn C. C. *Redox Rep.* 1997. 3–15.
59. Klebanoff S. J., Leukocyte J., *Biol.* 2005, 77, 598–625.
60. Zhang R., Brennan M. L., Shen Z., MacPherson J. C., Schmitt D., Molenda C. E., Hazen S. L. *J. Biol Chem.* 2002, 277, 46116–46122.
61. Winterbourn C. C. *Nat. Chem. Biol.* 2008, 4, 278–286.
62. Pullar J. M., Vissers M. C., Winterbourn. *IUBMB Life.* 2000, 50, 259–266.
63. Kettle A. J., Chan T., Osberg I., Senthilmohan R., Chapman A. L., Mocatta T. J., Wagener J. S. *Am. J. Respir Crit Care Med.* 2004, 170, 1317–1323.
64. Hazen S. L., Heinecke J. W., *J. Clin Invest.* 1997, 99, 2075–2081.
65. Rudolph V., Andrie R. P., Rudolph T. K., Friedrichs K., Klinke A., Hirsch-Hoffmann B., Schworer A. P., Lau D., Fu X., Klingel K., Sydow K., Didié M., Seniuk A., von Leitner E. C., Szoecs K., Schrickel Treede J. W. H., Wenzel U., Lewalter T., Nickenig G., Zimmermann W. H., Meinertz T., Boger R. H., Reichenspurner H., Freeman B. A., Eschenhagen T., Ehmke H., Hazen S. L., Willems S., Baldus S. *Nat. Med.* 2010, 16, s 470–474.

\*\*\*\*\*